Generalized mechanism of the resistance switching in binary-oxide-based resistive random-access memories

Katsumasa Kamiya,[1,*] Moon Young Yang,[1] Takahiro Nagata,[2] Seong-Geon Park,[3] Blanka Magyari-Köpe,[3] Toyohiro Chikyow,[2] Keisaku Yamada,[1] Masaaki Niwa,[1] Yoshio Nishi,[3] and Kenji Shiraishi[1]

[1]*Graduate School of Pure and Applied Sciences, University of Tsukuba, 1-1-1 Tennodai, Tsukuba, Ibaraki, 305-8571, Japan*

[2]*International Center for Materials Nanoarchitectonics, National Institute for Materials Science, 1-1 Namiki, Tsukuba, Ibaraki 305-0044, Japan*

[3]*Department of Electrical Engineering, Stanford University, Stanford, California 94305, USA*

(Received 6 November 2012; published 8 April 2013)

We report that V_O cohesion-isolation transition caused by carrier injection/removal is a generalized resistance switching mechanism of binary-oxide-based resistive random-access memories (ReRAMs). We propose universal guiding principles by which ReRAM with unipolar and bipolar operations can be designed by controlling electrode work functions. We found by first-principles calculations that structural phase transition with V_O cohesion-isolation is the physical origin of the resistance switching mechanism of binary-oxide-based ReRAM. Based on our theory, we can propose a guiding principle toward bipolar switching ReRAM with stable high work function metal electrodes.

DOI: 10.1103/PhysRevB.87.155201 PACS number(s): 77.84.Bw, 71.15.Mb

I. INTRODUCTION

Binary metal oxides are known to be a material exhibiting nonvolatile resistance switching by an applied electric filed.[1–3] With the advance of oxide nanotechnologies, its practical application for memory devices, so-called resistive random-access memories (ReRAMs), has recently emerged.[4–6] The ReRAM has a capacitorlike structure with a metal/oxide/metal stack, and switches between low- and high-resistance states with the application of short voltage pulses. Because the device has the excellent scaling merit as well as its high-speed and low-power operations, it has attracted increased attention as a promising candidate for the next generation nonvolatile memories.[7–10] Thus, clarification of the resistance switching in ReRAMs is not only imperative to realize high-quality ReRAMs, but also important to advance oxide-material sciences.[11,12]

The ON-OFF switching mechanism in binary-oxide-based ReRAM is, however, not fully elucidated. The resistance switching in the ReRAM is phenomenologically categorized into two modes; the switching is dependent (bipolar) or independent (unipolar) on the polarity of an applied voltage. More microscopically, it has been pointed out both experimentally and theoretically in TiO_2-based ReRAMs that the ON-OFF switching is governed by the formation and disruption of conducting filaments of oxygen vacancies (V_O).[13,14] Very recently, the same type of switching mechanism has been suggested experimentally for HfO_2-ReRAMs.[16] Yet, the main factors of the V_O-filament creation disruption and the mechanism of the electrode dependency of the bipolar and unipolar switching in such binary-oxide ReRAMs are still unclear.

In our previous works, it has been proposed that oxygen vacancy cohesion isolation upon carrier injection/removal is a strong driving force in the ON-OFF switching of TiO_2-based ReRAM.[15] The aim of this study is, in contrast, to verify whether or not the V_O cohesion-isolation process is related to inherent properties of V_O appearing in other binary oxides, and thus generalized to binary-oxide-based ReRAMs. We here focus on HfO_2, because it has been shown to exhibit good ReRAM behavior[16–27] as well as excellent compatibility with silicon technology; moreover, HfO_2 has the conduction band offset on Si larger than 1 eV,[28] showing high insulating property as compared with TiO_2. Our density functional theory (DFT) calculations demonstrated that V_O in both HfO_2 and TiO_2 shows the same type of a reversible cohesion-isolation transition that can be controlled by carrier injection and removal, indicating a common physics related inherently to the V_O properties in binary oxides. Based on these results, we found the importance of the matching between the V_O levels and Fermi levels of electrodes for effective carrier injection and removal, giving a general guideline for the realization of the desirable bipolar switching of binary-oxide-based ReRAMs.

II. CALCULATION METHODS

To study the properties of a monovacancy, we used one V_O in $2 \times 2 \times 2$ of a 12-atom unit cell of cubic HfO_2, hereafter indicated as the isolated-V_O model [Fig. 1(a)]. To simulate the ON and OFF states in HfO_2 based ReRAMs, we considered three different V_O configurations in the vacancy model, constructed by introducing four V_O into a 96-atom supercell of cubic HfO_2; (1) the V_O-chain model [Fig. 1(b)], (2) the partial-V_O-chain model [Fig. 1(c)], and (3) the disrupted-V_O-chain model [Fig. 1(d)]. The first model involves an ordered V_O filament, where a conductive channel is formed, corresponding to the ON state. The conductive channel is partially and fully ruptured in the second and last model, respectively, corresponding to the OFF state. The 96-atom supercell was constructed with three primitive vectors of $\mathbf{a}_1 = 2\sqrt{2}a(\cos 45^\circ \hat{\mathbf{x}} - \sin 45^\circ \hat{\mathbf{y}})$, $\mathbf{a}_2 = \sqrt{2}a(\sin 45^\circ \hat{\mathbf{x}} + \cos 45^\circ \hat{\mathbf{y}})$, and $\mathbf{a}_3 = 2a\hat{\mathbf{z}}$. The cell parameter a of 4.99 Å was optimized for the 12-atom unit cell, which is in good agreement with the experimental value of 5.08 Å. All calculations were performed using DFT within the local-density approximation (LDA), as implemented in the Vienna *ab initio* simulation package code.[29–31] It has been recently pointed out that quantitative description of V_O by DFT requires more accurate exchange-correlation functionals

 ©2013 American Physical Society

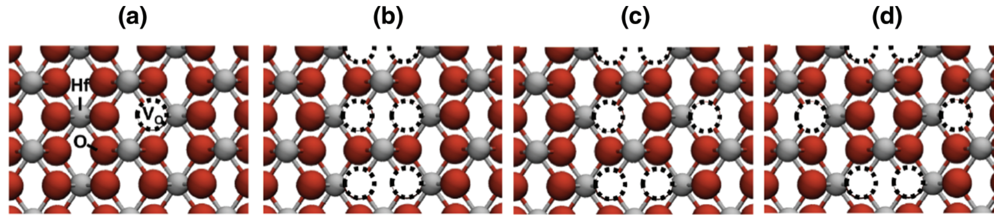

FIG. 1. (Color online) Atomistic structures of the (a) isolated-V_O, (b) V_O-chain, (c) partial-V_O-chain, and (d) disrupted-V_O-chain models in cubic HfO_2.

than LDA.[32,33] However, the use of the LDA could provide a qualitatively reasonable description of the V_O. For example, all of the LDA and other functionals show that an isolated V_O takes 2+ charge state for a wide range of the Fermi energy. A quantitative error by using LDA is estimated to be about 20% in terms of the formation energy of neutral oxygen vacancy. Taking into account this change, the resulting cohesive energy for V_O [defined by Eq. (1), see below], however, would still be qualitatively describing the stability transition as a function of the charge state, since the values are still larger than a typical DFT calculation error of tens of meV. Furthermore, the characteristic feature of the electronic structure for the V_O-chain model was also confirmed by the LDA with the addition of the on-site Coulomb corrections (LDA + U) method.[34] Therefore, the use of LDA could not change qualitative features of the physics of the vacancy cohesion-isolation transition upon carrier injection/removal, discussed in this study.

The valence configurations of the pseudopotentials are $5p^6 5d^2 6s^2$ for Hf and $2s^2 2p^4$ for O. We used the projector-augmented-wave pseudopotentials with a plane wave cutoff energy of 37 Ry. Monkhorst-Pack k-point sets of $2 \times 2 \times 2$ and $2 \times 4 \times 4$ were used for the isolated-V_O model and the other three models, respectively. After the geometry optimizations, all the atomic forces were less than 0.005 eV/Å.

III. RESULTS AND DISCUSSION

Figure 2(a) displays cohesive energy $E_c(q)$ per one V_O as a function of charge state q for the V_O-chain model with respect to the isolated-V_O model, defined as

$$E_c(q) = \frac{1}{4}\left\{E\left(V_O^q\text{-chain}\right) + 3 \times E(\text{bulk}) - 4 \times E\left(\text{isolated-}V_O^q\right)\right\}, \quad (1)$$

where $E(V_O^q\text{-chain})$ and $E(\text{isolated-}V_O^q)$ are the total energy of the V_O-chain model and the isolated-V_O model in charge state q, respectively. $E(\text{bulk})$ is the total energy of HfO_2 bulk crystal, and the factors 3 and 4 are used because the V_O-chain model has four V_O in the supercell.

We found in Fig. 2(a) that $E_c \leqslant 0$ for the V_O-chain model with $q = 0$ and 1+. This trend is exactly the same as in the case of rutile TiO_2, as reported in our previous work.[15] Furthermore, the calculated cohesive energy is −0.6 eV and −0.3 eV per one V_O for 0 and 1+ charge states, respectively, which are also comparable with that for rutile TiO_2, −0.9 eV and −0.5 eV for 0 and 1+ charge states, respectively.[15] These results indicate clearly that V_Os undertake cohesion-isolation transition by carrier injection and removal, which is universal phenomena in both HfO_2 and TiO_2.

The V_O cohesion-isolation transition is also observed in the formation energy diagram of HfO_2 as a function of the Fermi energy E_F [Fig. 2(b)]. The formation energy for the system involving n oxygen vacancies in charge state q, $E_{\text{form}}(nV_O^q)$, was calculated using the following formula:[35]

$$E_{\text{form}}\left(nV_O^q\right) = \left[E\left(nV_O^q\right) + E(\text{bulk}^0)\right] - \left[E\left(nV_O^0\right) + E(\text{bulk}^{nq})\right] + nqE_F + \frac{3(nq)^2}{10\epsilon r_0}, \quad (2)$$

where $E(nV_O^q)$ is the total energy of crystal containing n oxygen vacancies in charge state q, and $E(\text{bulk}^{nq})$ is the total energy of HfO_2 bulk crystal in charge state nq. The last term is a background charge correction proposed by Blöchl,[36] where ϵ of 20 is the relative permittivity for cubic HfO_2, and r_0 of 6.19 Å is the radius of a sphere of the same volume as the supercell.

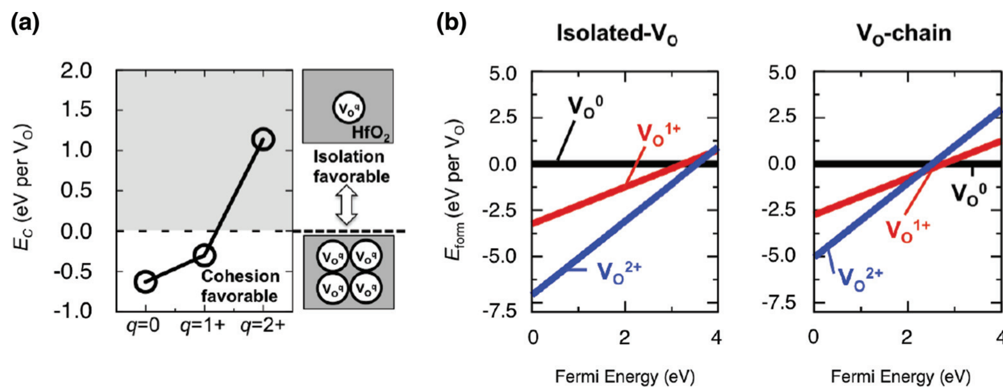

FIG. 2. (Color online) (a) V_O cohesive energy as a function of charge state q for the V_O-chain model with respect to the isolated-V_O model, and (b) formation energy diagram per one V_O for the isolated-V_O and V_O-chain models as a function of Fermi energy.

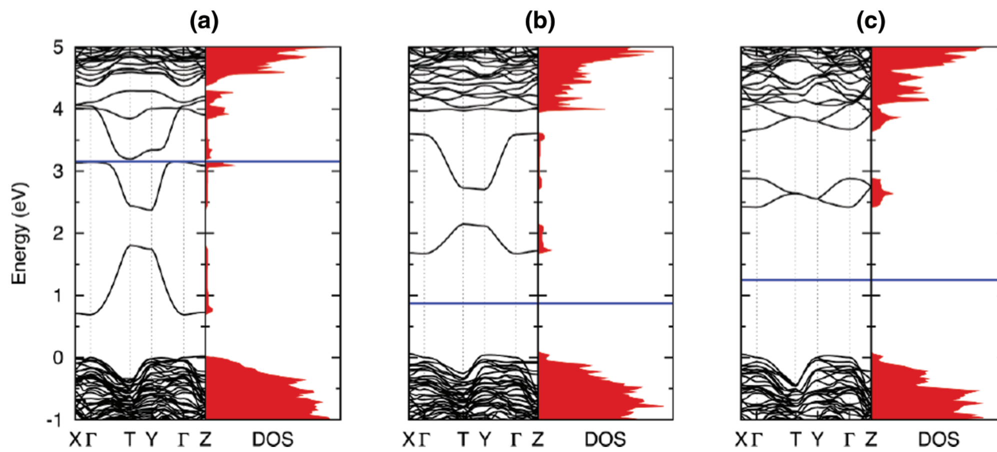

FIG. 3. (Color online) Energy band structures and density of states for the (a) V_O-chain model in the one-electron-captured state, (b) partial-V_O-chain model in the intrinsic state, and (c) disrupted-V_O model in the intrinsic state. The horizontal lines indicate the position of the Fermi level. DOS is shown in arbitrary units.

We found in Fig. 2(b) that an isolated V_O takes the 2+ charge state [intrinsic state (V_O^{2+})]. However, when V_O form a cohesive chain, the one- and two-electron-captured states ($V_O^{1+}$and V_O^{0}) become energetically favorable in the V_O-chain model for the upper range of the Fermi energy, i.e., $E_F \geqslant 2$ eV. This energy range is expected to be in the Si band gap region, because the Si valence band offset can be estimated to be 2.3 eV on HfO_2 valence band top.[37] These results clearly indicate that the energetics of the V_O cohesion-isolation transition depend on the V_O charged states. The similar charge-state dependency has also been confirmed in TiO_2.[15]

A detailed analysis of the electronic structures of HfO_2 reveals two significant roles of electrons injected into V_O in the cohesion-isolation transition. Figure 3(a) shows the electronic energy bands and density of states (DOS) for the V_O-chain model. We found that defect energy levels have a significant dispersion only along the Γ-T/Y lines. Obviously, this large dispersion is ascribed to the formation of the [010] ordered V_O-chain [Fig. 1(b)]. It is thus believed from this band structure that the V_O-chain model corresponds to the ON state (metallic). In sharp contrast, when one V_O is isolated from the chain [Fig. 1(c)], the amount of the band dispersion becomes smaller than that in the V_O-chain model [Fig. 3(b)]. This trend is enhanced further by the isolation of two V_O from the chain (the filament disruption) [Figs. 1(d) and 3(c)]. These band structures show the insulating feature, corresponding to the OFF state.

Figure 4 shows partial DOS of d orbitals of aligned Hf atoms for the three V_O configurations. It can be seen that the Hf d orbitals form the V_O conducting channel bands. The figure also shows representative partial charge densities corresponding to the bands. We see that the defect states have a character of Hf d orbitals parallel to the ⟨010⟩ direction. These d orbitals form an electron conduction path in a V_O chain [Figs. 4(a) and 4(b)], but it can be broken easily by V_O isolation [Fig. 4(c)]. In the perfect V_O-chain case [Fig. 4(a)], four O^{2-} ions are coordinated to one Hf^{4+} ion and form a square planer (the xy plane) [Fig. 1(b)]; five d orbitals are spitted into the energetically lower d_{z^2}, d_{yz}, and d_{zx} orbitals, and the energetically higher $d_{x^2-y^2}$ and d_{xy} orbitals due to the crystal field. The former three d states can contribute to the hybridization in successive Hf ions, leading to the formation of bonding and antibonding states [upper inset in Fig. 4(a)]. The bonding orbitals are eventually occupied in the cases of

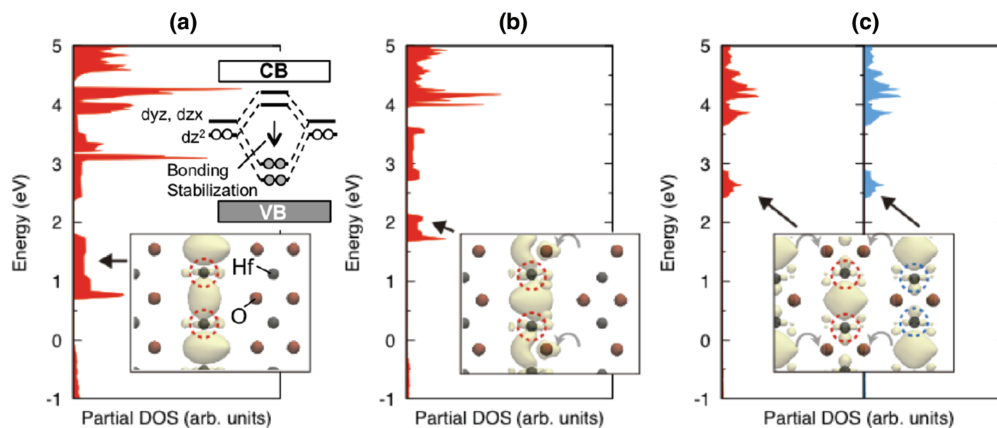

FIG. 4. (Color online) Partial density of states (PDOS) of d orbitals in aligned Hf atoms for the three V_O configurations. The panels (a)–(c) correspond to the ones shown in Fig. 3. The insets show the representative partial charge densities of defect states; the Hf ions for PDOS are highlighted by dotted circles, and moved O atoms are indicated by arrows. The upper inset in the panel (a) is a schematic picture of d hybridization.

the one-electron captured and two-electron captured states, thereby leading to a larger amount of electron energy gain.

In addition to this band energy gain, electron injection into the positively charged V_O cohesive filament also reduces the Coulomb repulsion between ordering Hf^{4+} ions. When V_O is isolated in HfO_2, positively charged Hf^{4+} ions can move outward to reduce their Coulomb repulsion, leading to the stabilization of the intrinsic V_O^{2+} state. When V_Os form a cohesive filament, the previously mentioned outward displacement of Hf^{4+} ions are strongly suppressed due to the geometrical restriction caused by an ordered V_O cohesive filament structure. Thus, electrons should be incorporated to neutralize the positively charged V_O cohesive filament for reducing the repulsive Coulomb energy.

Binary oxides such as HfO_2, TiO_2, and Al_2O_3 are characterized by their ionic bonding and coordination number that are strongly related to defect concentration in the materials.[38,39] HfO_2 is a material that has both higher ionic character of the bonding and higher atomic coordination numbers. If a defect is created in this compound, it is thus not easily able to relax to remove the defect. The nonequilibrium concentration of defects is, therefore, high in HfO_2.[39] The present study clearly shows that such existing V_O are able to be condensed and dispersed by V_O cohesion-isolation transition induced by electron injection and removal. It has been recently shown by our previous works that the same mechanism takes place even in other types of binary oxides such as TiO_2 and Al_2O_3.[15,40,41] TiO_2 is a nonstoichiometric compound where the equilibrium concentration of nonstoichiometric defects is naturally high. On the other hand, Al_2O_3 has both lower bond ionicity and lower coordination numbers than those of HfO_2 and TiO_2, and it is thus known as a poor V_O former. Combining the results from the present and previous works provides a comprehensive picture for the switching mechanism for binary-oxide-based ReRAM operation, where the V_O cohesion-isolation transition triggered by electron injection and removal generally occurs if V_O are created in these binary oxides.

It is worthwhile to note the energetics of the V_O cohesion-isolation transition in binary oxide, versus the energy scale of applied voltage. As stated above, the calculated V_O cohesive energy for both HfO_2 and TiO_2 is on the order of 1 eV per V_O. This value is comparable to the typical energy scale in binary-oxide-based ReRAMs, i.e., the order of $\sim$1 eV which is estimated from the typical value for applied voltage of the ReRAMs, $\sim$1 V. Thus, we conclude that the electron injection and removal by applying electric field can induce the V_O cohesion-isolation transition via the generalized mechanism, thereby being one of the main driving factors responsible for binary-oxide-based ReRAM operation.

How electrons are injected into V_O in binary oxide is one of the crucial factors that determines a switching mechanism of ReRAMs. We have already proposed that bipolar or unipolar behavior is determined by how the carriers are injected into V_O.[15] In this theory, when the system Fermi level is well matched with V_O defect levels, both electron injection and removal occur via electrodes [Figs. 6(a) and 6(b) in Ref. 15], leading to a bipolar operation. On the other hand, if the system Fermi level is not matched with V_O defect levels, electrons can be injected only from the filament [Fig. 6(c) in Ref. 15].

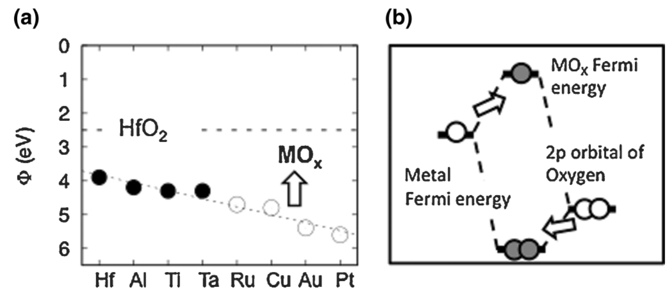

FIG. 5. (a) Work function for typical top electrodes (TE) of TE/HfO_2/TiN-ReRAMs. Solid and open circles indicate experimentally observed bipolar and unipolar operation, respectively. The data of work function are taken from Ref. 42. The arrow in the figure illustrates work function modulation of electrodes by bond engineering. (b) Hybridization of metal and oxygen orbitals. The closed circles represent occupation by electrons.

Based on this theory, low work function metals are suitable for bipolar operation, since typical V_O levels are around 4.0 eV from the vacuum level. This is schematically shown in the universal diagram (Fig. 5), where work function for typical top electrodes (TE) of TE/HfO_2/TiN-ReRAMs are plotted according to experimentally determined bipolar and unipolar behaviors.[17–21,23,26] This diagram indicates that high-reactivity metals (Hf, Al, Ti, and Ta) are suitable for bipolar operation, but low-reactivity (stable) metals such as Ru, Cu, Au, and Pt are appropriate to unipolar operation. Based on this figure, we propose a guideline to realize bipolar switching ReRAM with high work function metal electrodes. Recently, bipolar operation was observed even in ReRAMs with stable high work function metal electrodes such as Cu and Pt.[22,24] Moreover, Pt-O bonds are really observed by HX-PES.[22] It is well known that partial oxidation lowers the metal work function, since high-energy antibonding levels are occupied by electrons [the inset in Fig. 5]. Accordingly, we can propose a guiding principle toward high quality bipolar switching ReRAM; bond-engineering such as metal-O bond formations can sufficiently modify work function of metal electrodes, leading to the bipolar operation in ReRAM with stable high work function metal electrodes.

IV. CONCLUSION

In conclusion, our DFT calculations have clarified that structural phase transition with V_O cohesion-isolation is the physical origin of the ON-OFF switching mechanism of binary-oxide-based ReRAM. Based on our theory, we can propose a guiding principle toward bipolar switching ReRAM with stable high work function metal electrodes.

ACKNOWLEDGMENTS

Computations were performed on a NEC SX-9 at the Institute for Solid-State Physics, The University of Tokyo, and a Fujitsu PrimeQuest at the Research Center for Computational Science, Okazaki Research Facilities, National Institutes of Natural Sciences. This research was supported by a Grant-in-Aid for Young Scientists (B) (No. 22740259) from the Japan Society for the Promotion of Science.

*kkamiya@comas.frsc.tsukuba.ac.jp

[1] T. W. Hickmott, J. Appl. Phys. **33**, 2669 (1962).
[2] G. Dearnaley, A. M. Stoneham, and D. V. Morgan, Rep. Prog. Phys. **33**, 1129 (1970).
[3] J. F. Gibbons and W. E. Beadle, Solid-State Electron. **7**, 785 (1964).
[4] W. W. Zhuang, W. Pan, B. D. Ulrich, J. J. Lee, L. Stecker, A. Burmaster, D. R. Evans, S. T. Hsu, M. Tajiri, A. Shimaoka, K. Inoue, T. Naka, N. Awaya, A. Sakiyama, Y. Wang, S. Q. Liu, N. J. Wu, and A. Ignatiev, in *Electron Devices Meeting, 2002 (IEDM)* (IEEE, New York, 2002), pp. 193–196.
[5] T. Sakamoto, H. Sunamura, H. Kawamura, H. Hasegawa, T. Nakayama, and M. Aono, Appl. Phys. Lett. **82**, 3032 (2003).
[6] I. G. Baek, M. S. Lee, S. Seo, M.-J. Lee, D. H. Seo, D.-S. Suh, J. C. Park, S. O. Park, T. I. Kim, I. K. Yoo, U-In Chung, and J. T. Moon, in *Electron Devices Meeting, 2004 (IEDM)* (IEEE, New York, 2004), pp. 587–590.
[7] R. Waser and M. Aono, Nat. Mater. **6**, 833 (2007).
[8] A. Sawa, Mater. Today **11**, 28 (2008).
[9] H. Akinaga and H. Shima, Proc. IEEE **98**, 2237 (2010).
[10] Y. Nishi, Curr. Appl. Phys. Lett. **11**, e101 (2011).
[11] E. Dagotto, Science **309**, 257 (2005).
[12] H. Takagi and H. Y. Hwang, Science **327**, 1601 (2010).
[13] D.-H. Kwon, K.-M. Kim, J.-H. Jang, J.-M. Jeon, M.-H. Lee, G.-H. Kim, X.-S. Li, G.-S. Park, B. Lee, S. Han, M. Kim, and C.-S. Hwang, Nat. Nanotech. **5**, 148 (2010).
[14] S.-G. Park, B. M.-Köpe, and Y. Nishi, in *IEEE Symposium on VLSI Technology* (IEEE, New York, 2011), pp. 46–47.
[15] K. Kamiya, M. Y. Yang, S-G. Park, B. Magyari-Köpe, Y. Nishi, M. Niwa, and K. Shiraishi, Appl. Phys. Lett. **100**, 073502 (2012).
[16] C. Cagli, J. Buckley, V. Jousseaume, T. Cabout, A. Salaun, H. Grampeix, J. F. Nodin, H. Feldis, A. Persico, J. Cluzel, P. Lorenzi, L. Massari, R. Rao, F. Irrera, F. Aussenac, C. Carabasse, M. Coue, P. Calka, E. Martinez, L. Perniola, P. Blaise, Z. Fang, Y. H. Yu, G. Ghibaudo, D. Deleruyelle, M. Bocquet, C. Muller, A. Padovani, O. Pirrotta, L. Vandelli, L. Larcher, G. Reimbold, and B. De Salvo, in *Electron Devices Meeting, 2011 (IEDM)* (IEEE, New York, 2011), pp. 28.7.1–28.7.4.
[17] H-Y. Lee, P-S. Chen, C-C. Wang, S. Maikap, P-J. Tzeng, C-H. Lin, L-S. Lee, and M-J. Tsai, Jpn. J. Appl. Phys. **46**, 2175 (2007).
[18] H. Y. Lee, P. S. Chen, T. Y. Wu, C. C. Wang, P. J. Tzeng, C. H. Lin, F. Chen, M-J. Tsai, and C. Lien, Appl. Phys. Lett. **92**, 142911 (2008).
[19] H. Y. Lee, P. S. Chen, T. Y. Wu, Y. S. Chen, C. C. Wang, P. J. Tzeng, C. H. Lin, F. Chen, C. H. Lien, and M.-J. Tsai, in *Electron Devices Meeting, 2008 (IEDM)* (IEEE, New York, 2008), pp. 1–4.
[20] Ch. Walczyk, Ch. Wenger, R. Sohal, M. Lukosius, A. Fox, J. Dąbrowski, D. Wolansky, B. Tillack, H.-J. Müssig, and T. Schroeder, J. Appl. Phys. **105**, 114103 (2009).
[21] Y. S. Chen, H. Y. Lee, P. S. Chen, P. Y. Gu, C. W. Chen, W. P. Lin, W. H. Liu, Y. Y. Hsu, S. S. Sheu, P. C. Chiang, W. S. Chen, F. T. Chen, C. H. Lien, and M.-J. Tsai, in *Electron Devices Meeting, 2009 (IEDM)* (IEEE, New York, 2009), pp. 1–4.
[22] M. Haemori, T. Nagata, and T. Chikyow, Appl. Phys. Express **2**, 061401 (2009).
[23] P-S. Chen, H-Y. Lee, Y-S. Chen, F. Chen, and M-J. Tsai, Jpn. J. Appl. Phys. **49**, 04DD18 (2010).
[24] T. Nagata, M. Haemori, Y. Yamashita, H. Yoshikawa, Y. Iwashita, K. Kobayashi, and T. Chikyow, Appl. Phys. Lett. **97**, 082902 (2010).
[25] T. Nagata, M. Haemori, Y. Yamashita, H. Yoshikawa, Y. Iwashita, K. Kobayashi, and T. Chikyow, Appl. Phys. Lett. **99**, 223517 (2011).
[26] T. Bertaud, D. Walczyk, Ch. Walczyk, S. Kubotsch, M. Sowinska, T. Schroeder, Ch. Wenger, C. Vallée, P. Gonon, C. Mannequin, V. Jousseaume, and H. Grampeix, Thin Solid Films **520**, 4551 (2012).
[27] Y. S. Chen, H. Y. Lee, P. S. Chen, C. H. Tsai, P. Y. Gu, T. Y. Wu, K. H. Tsai, S. S. Sheu, W. P. Lin, C. H. Lin, P. F. Chiu, W. S. Chen, F. T. Chen, C. Lien, and M.-J. Tsai, in *Electron Devices Meeting, 2011 (IEDM)* (IEEE, New York, 2011), pp. 31.3.1–31.3.4.
[28] J. Robertson, J. Vac. Sci. Technol. B **18**, 1785 (2000).
[29] P. Hohenberg and W. Kohn, Phys. Rev. **136**, B864 (1964).
[30] W. Kohn and L. J. Sham, Phys. Rev. **140**, A1133 (1965).
[31] G. Kresse and J. Hafner, Phys. Rev. B **49**, 14251 (1994).
[32] J. L. Lyons, A. Janotti, and C. G. Van de Walle, Microelectron. Eng. **88**, 1452 (2011).
[33] R. Gillen, J. Robertson, and S. J. Clark, Appl. Phys. Lett. **101**, 102904 (2012).
[34] B. Magyari-Köpe and Y. Nishi (unpublished).
[35] K. Yamaguchi, A. Otake, K. Kamiya, Y. Shigeta, and K. Shiraishi, Jpn. J. Appl. Phys. **50**, 04DD05 (2011).
[36] P. E. Blöchl, Phys. Rev. B **62**, 6158 (2000).
[37] We assumed that conduction band offset on Si for HfO_2 is 1.5 eV, according to Ref. 28. The corresponding valence band offset is thus 3.4 eV. Considering the systematic gap narrowing by DFT-LDA, we simply multiplied these values by the ratio of the calculated band gap, 4 eV, and the experimental one, 6 eV, for HfO_2.
[38] G. Lucovsky, J. Vac. Sci. Technol. A **19**, 1553 (2001).
[39] J. Robertson, Solid-State Electronics **49**, 283 (2005).
[40] K. Kamiya, M. Y. Yang, B. Magyari-Köpe, M. Niwa, Y. Nishi, and K. Shiraishi, in *Electron Devices Meeting, 2012 (IEDM)* (IEEE, New York, 2012), pp. 20.2.1–20.2.4.
[41] M. Y. Yang, K. Kamiya, B. Magyari-Köpe, H. Momida, T. Ohno, M. Niwa, Y. Nishi, and K. Shiraishi, Jpn. J. Appl. Phys. (to be published).
[42] *CRC Handbook of Chemistry and Physics*, edited by D. R. Lide, 89th ed. (CRC, Boca Raton, FL, 2008).